

Received March 22, 2018, accepted April 22, 2018, date of publication May 7, 2018, date of current version June 19, 2018.

Digital Object Identifier 10.1109/ACCESS.2018.2833290

# Attitude Estimation Fusing Quasi-Newton and Cubature Kalman Filtering for Inertial Navigation System Aided With Magnetic Sensors

HAOQIAN HUANG<sup>1</sup>, JUN ZHOU<sup>1</sup>, (Member, IEEE), JUN ZHANG<sup>2</sup>, (Member, IEEE), YUAN YANG<sup>2</sup>, RUI SONG<sup>2</sup>, JIANFENG CHEN<sup>3</sup>, AND JIAJIN ZHANG<sup>4</sup>

<sup>1</sup>College of Energy and Electrical Engineering, Hohai University, Nanjing 210098, China

<sup>2</sup>School of Instrument Science and Engineering, Southeast University, Nanjing 210096, China

<sup>3</sup>School of Automotive and Traffic Engineering, Jiangsu University, Zhenjiang 212013, China

<sup>4</sup>Fujian Provincial Key Laboratory of Coast and Island Management Technology Study, Fujian Institute of Oceanography, Xiamen 361013, China

Corresponding author: Haoqian Huang (hquang@hhu.edu.cn)

This work was supported in part by the National Natural Science Foundation of China under Grant 61703098, Grant 61573001, Grant 61403079, Grant 61601123, Grant 51405203, and Grant 41449904, in part by the Natural Science Foundation of Jiangsu Province under Grant BK20160699 and Grant BK20160696, in part by the Fundamental Research Funds for the Central Universities under Grant 2017B07214, in part by the China Postdoctoral Science Foundation under Grant 2016M601727, in part by the Six Talent Peaks Project in Jiangsu Province under Grant 2016-JXQC-007, and in part by the Voyage of Scientific Investigation and Experimental Study of Taiwan Strait in 2015.

**ABSTRACT** In the complex underwater environment, the performance of microelectro-mechanical system sensors is degraded sharply and the errors will become much larger. Especially when the magnetic sensor is disturbed by the external magnetic interference, the measurements become unobservable so that the navigation information is estimated erroneously. To solve this problem, the paper proposes a novel method fusing Quasi-Newton and cubature Kalman filter (QNCKF). This method takes full advantage of the computation efficiency of the Quasi-Newton and the estimation accuracy of CKF in the case of nonlinearity. The performance of QNCKF is verified theoretically and evaluated by experiments. The results indicate that when the magnetic sensor is interfered, QNCKF and CKF still can maintain high estimation accuracy, whereas the extended Kalman filter performs poorly. Moreover, QNCKF is superior to CKF in the aspect of computational efficiency. Therefore, QNCKF has the highest priority in terms of estimation accuracy and computational efficiency among the three methods and it is more suitable to be applied to the underwater gliders than the other two methods.

**INDEX TERMS** Underwater glider, inertial navigation, magnetic sensor, Quasi-Newton, magnetic interference, attitude estimation.

## I. INTRODUCTION

With active position control capability, underwater gliders have obvious advantages over the profiling floats in the ocean applications. An underwater glider can perform the saw-tooth trajectories from the surface to the depths of 1000-1500m. The trajectories are reprogrammable by using bidirectional communication via satellites on the surface. The forward speed of the glider can reach up to 40km per day. A glider can be operated with the help of wings for a few months before being recovered [1]–[5]. Despite these merits, there are still some difficulties for the real application of underwater gliders. One of them is the inherently large propagation errors of the navigation system applied to underwater gliders. This problem is presented for nearly all underwater vehicles.

Just in a few meters below the surface of water, no reference signals, such as Global Positioning System (GPS), can be used to correct the navigation system errors [6], [7].

Perhaps different from any other unattended observing platforms, a glider has the most stringent constraints for the types of sensors which it can carry [8], [9]. Advances in Micro-Electro-Mechanical System (MEMS) technologies have brought significant developments in low-cost strap-down inertial navigation systems (SINSs) [10]–[12]. Since the weight or the cost is an important issue in application of navigation systems, the heavy inertial sensors with low accuracy are excluded or substituted, and the low-cost systems like MEMS-grade accelerometers and gyroscopes are better applied to gliders. Nevertheless, the navigation errors

of the low-cost inertial measurement unit (IMU) intensively increase over time due to sensor noises, drifts and biases of the MEMS-grade IMU [13]–[15]. The IMU contains tri-axis magnetic sensors to measure Earth's magnetic field, and it is used to correct the heading calculated by gyroscopes [16]. The inertial navigation system (INS) integrated with the dead reckoning (DR) can effectively estimate the navigation information of gliders [17].

Usual deployment durations are anywhere from 1 to 6 months, and at horizontal speeds of about 0.25m/s, ranges of over 3000 km can be achieved. A typical glider dive will flight from the surface to the depth of 1000m and return in 6h approximately, covering 6km horizontally in that period of time [18]. The performance of the glider can be affected by the ocean parameters. The upper ocean responds to the monsoon, with a deep (~200 m) mixed layer (ML) in the winter and a shallow (~30 m) ML in the summer [19]. The mixed layer depth (MLD) differs from tens of meters to hundreds of meters according to different season varieties, geographical locations and wind effects. MLD is susceptible to be influenced by the outside factors. Ocean environment with the depth of hundreds of meters has some characteristics, such as high spatiotemporal variation, higher current velocity, abrupt change of temperature and salinity, biological variety, boats with frequent coming and going and so on. Therefore, ocean parameters change frequently and abruptly [20]. An underwater glider can move up and down in a water column [21]. It glides in different depths and wide ranges. Thus, it must glide and go through the MLD. The dynamics of glider is changed by ocean parameter variations. The coupling errors of three axes for inertial measurement units obviously increase due to frequent pitch or roll motion [22]. Meanwhile, the change of dynamics also causes more errors of attitudes calculated by accelerations. The magnetic sensor carried on glider is vulnerable to be disturbed by high noises, orthogonal errors and offset errors. Moreover, barges around a glider, other underwater vehicles and other electromagnetic interferences also cause hard magnetic errors and soft magnetic errors, which make the accuracy of magnetic sensor measurement lower. The accuracy of attitude determination is decreased as these above factors.

Theoretically, we can determine a nonlinear inertial sensor system error model with an arbitrary order. The idea is motivated by the fact that models with higher order are supposed to offer the more accurate dynamics description of inertial sensor error. However, this is challenged by two shortcomings in practice: (1) the mathematical derivation is complex and time-consuming in computation; (2) the mathematical derivation may contain a number of terms, including terms with very low significance or influence in the nonlinear model [23]. It is hard to construct precise error model for the inertial system. Therefore, to improve the prediction accuracy, The suitable filter needs to be designed for attitude prediction [24].

The EKF maintains the computationally efficient updated form of the KF, but its major drawback is the negligence

for higher-order terms of nonlinear system function, leading to low accurate estimation [25]–[28]. When magnetic sensors are disturbed so that the measurements are low observable or even unobservable, the performance of EKF will degrade sharply and seriously in the high nonlinear case. The unscented Kalman filtering (UKF) employs a range of sigma-points to propagate the covariance matrix and states based on the deterministic sampling framework [29]–[33]. The sigma-points are generated for UKF through unscented transformation and UKF can be regarded as a second-order approximation when implemented with a nonlinear model [34]. Therefore, theoretically the estimation accuracy of UKF is higher than EKF in the complex underwater application, especially in the cases with higher nonlinearity [35]–[39]. Different from UKF which makes use of  $2n + 1$  unscented points to produce the covariance matrix and state, the cubature Kalman filter (CKF) propagates the covariance matrix and the state with  $2n$  cubature points. The computational burden of CKF is relatively lower than UKF when UKF and CKF perform the same matrix decomposition methods like Cholesky method or singular value decomposition. The CKF performs better than the UKF in stability, particularly when the dimension of the system is higher than three [40]–[44]. The MEMS inertial sensor has large errors due to its inherent characteristics. The harsh and complex environment causes the errors of MEMS sensors much larger. The improvement of attitude estimation accuracy is still a problem, especially under the condition of magnetic interference, which leads to unobservable or weakly observable measurements. In such a case, the performance of traditional linear method degrades. The CKF has the better estimation accuracy even if measurements become unobservable, but the computational burden of CKF is much higher than EKF. The paper proposes a novel method fusing Quasi-Newton and CKF (QNCKF) which makes fully use of the anti-interference advantage and the computational efficiency to obtain high accuracy navigation information for a long period of gliding.

The structure of this paper is shown as follows. Section 2 introduces the QNCKF and proves the convergence and stability of the proposed algorithm. Section 3 shows a notable improvement in the performance of the proposed algorithm over the EKF and the CKF with a series of experiments. Finally, Section 4 summarizes the main conclusions and results of this paper.

## II. MODEL AND ALGORITHM

### A. PROBLEM STATEMENT

The considered nonlinear discrete-time system is represented by:

$$\mathbf{X}_{k|k} = f(\mathbf{X}_{k-1|k-1}) + \mathbf{W}_{k-1} \quad (1)$$

$$\mathbf{Z}_{k|k} = h(\mathbf{X}_{k|k}) + \mathbf{V}_k \quad (2)$$

where  $\mathbf{X}_{k|k}$ , as shown in Eq. (3), is the state vector at the moment  $k$ ;  $\mathbf{X}_{k-1|k-1}$  is the state vector at the moment  $k - 1$ ;  $\mathbf{Z}_{k|k}$  is the ideal measurement vector;  $f$  and  $h$  are the

nonlinear functions;  $\mathbf{W}_{k-1}$  and  $\mathbf{V}_k$  are the uncorrelated zero-mean Gaussian white noises [45]–[47].

$$\mathbf{X} = [\delta\mathbf{P} \ \delta\mathbf{V} \ \phi \ \nabla \ \varepsilon \ \delta\mathbf{A}]^T \quad (3)$$

where  $\delta\mathbf{P} = (\delta L \ \delta\lambda \ \delta h)^T$ ;  $\delta\mathbf{V} = (\delta V_E \ \delta V_N \ \delta V_U)$ ;  $\phi = (\phi_E \ \phi_U \ \phi_N)$ ;  $\nabla = (\nabla_{bx} \ \nabla_{by} \ \nabla_{bz})$ ;  $\varepsilon = (\varepsilon_{bx} \ \varepsilon_{by} \ \varepsilon_{bz})$ ;  $\delta\mathbf{A} = (\delta\varphi \ \delta\theta \ \delta\gamma)$ ;  $\delta L, \delta\lambda, \delta h$  are latitude, longitude and altitude errors;  $\delta V_E, \delta V_N, \delta V_U$  are velocity errors along east, north and upward directions;  $\phi_E, \phi_U, \phi_N$  are the orientation errors of the calculated platform represented in the local East-North-Upward coordinate frame;  $\nabla_{bx}, \nabla_{by}, \nabla_{bz}$  are the accelerometer biases in the three axes;  $\varepsilon_{bx}, \varepsilon_{by}, \varepsilon_{bz}$  are the gyroscope biases in three axes;  $\delta\varphi, \delta\theta, \delta\gamma$  are heading, pitch and roll errors.

The observation vector  $\mathbf{Z}$  is:

$$\mathbf{Z} = \begin{bmatrix} V_E^{INS} - V_E^{DR} \\ V_N^{INS} - V_N^{DR} \\ V_U^{INS} - V_U^{DR} \\ \text{-----} \\ \varphi^{Gyro} - \varphi^{Mag} \\ \theta^{Gyro} - \theta^{Acce} \\ \gamma^{Gyro} - \gamma^{Acce} \end{bmatrix} = \begin{bmatrix} \delta V_E^{INS} - \delta V_E^{DR} \\ \delta V_N^{INS} - \delta V_N^{DR} \\ \delta V_U^{INS} - \delta V_U^{DR} \\ \text{-----} \\ \delta\varphi^{Gyro} - \delta\varphi^{Mag} \\ \delta\theta^{Gyro} - \delta\theta^{Acce} \\ \delta\gamma^{Gyro} - \delta\gamma^{Acce} \end{bmatrix} \quad (4)$$

where  $V_E^{INS}, V_N^{INS}, V_U^{INS}$  are the velocities measured by INS;  $V_E^{DR}, V_N^{DR}, V_U^{DR}$  are the velocities estimated by DR; heading angle  $\varphi^{Gyro}$ , pitch angle  $\theta^{Gyro}$  and roll angle  $\gamma^{Gyro}$  are measured by the gyroscope, respectively;  $\varphi^{Mag}$  is heading is heading angle measured by the magnetometer;  $\theta^{Acce}, \gamma^{Acce}$  are pitch angle and roll angle measured by the accelerometer, respectively;  $\delta V_E^{INS}, \delta V_N^{INS}, \delta V_U^{INS}$  are the measurement errors of INS along the east, north and upward directions, respectively;  $\delta V_E^{DR}, \delta V_N^{DR}, \delta V_U^{DR}$  are the estimated errors by DR along the east, north and upward directions, respectively;  $\delta\varphi^{Gyro}, \delta\theta^{Gyro}, \delta\gamma^{Gyro}$  are the corresponding attitude error estimates by gyroscopes, respectively;  $\delta\varphi^{Mag}$  is the heading angle error measured by the magnetometer;  $\delta\theta^{Acce}, \delta\gamma^{Acce}$  are the pitch angle and the roll angle measured by accelerometers, respectively.

### B. PROPOSED ALGORITHM

The proposed QNCKF fully fuses the Quasi-Newton and CKF to perform better in terms of accuracy and computational efficiency. For the conventional CKF, the state transition function  $f(\mathbf{X}_{k-1|k-1})$  is expanded into Taylor series around the mean  $\bar{\mathbf{X}}_{k-1|k-1}$  of a random variable  $\mathbf{X}_{k-1|k-1}$ , but QNCKF can use Quasi-Newton to acquire the new iterative point and approach the state function as fast as possible. Subsequently, the QNCKF is continually implemented to achieve time update and measurement update. Ultimately, the state estimation is obtained not only more accurately but also more efficiently. The flow diagram of QNCKF is shown in Fig. 1 and the detailed interpretations are introduced in the following parts.

### 1) ALGORITHM FUSION AND ANALYSIS

A random variable  $\mathbf{X}_{k-1|k-1}$  with mean  $\bar{\mathbf{X}}_{k-1|k-1}$  and covariance matrix  $\mathbf{P}_{k-1|k-1}$  obeys a Gaussian distribution  $\mathbf{X}_{k-1|k-1} \sim N(\bar{\mathbf{X}}_{k-1|k-1}, \mathbf{P}_{k-1|k-1})$ . Define  $\Delta\mathbf{X}_{k-1|k-1}$  as  $\mathbf{X}_{k-1|k-1} - \bar{\mathbf{X}}_{k-1|k-1}$  with the Gaussian distribution  $\Delta\mathbf{X}_{k-1|k-1} \sim N(0, \mathbf{P}_{k-1|k-1})$ , and the state transition function  $f(\mathbf{X}_{k-1|k-1})$  can be extended by Quasi-Newton around iteration point  $\mathbf{X}_{k-1|k-1}$  [48], [49]:

$$f(\mathbf{X}_{k-1|k-1} + \delta) \approx q_{k-1|k-1}(\delta) = f(\mathbf{X}_{k-1|k-1}) + \nabla f(\mathbf{X}_{k-1|k-1})^T \delta + \frac{1}{2} \delta^T \nabla^2 f(\mathbf{X}_{k-1|k-1}) \delta \quad (5)$$

In order to avoid the use of Hessian Matrix, use a positive definite matrix  $\mathbf{B}_{k-1|k-1}$  to approximately substitute Hessian Matrix  $\nabla^2 f(\mathbf{X}_{k-1|k-1})$ .  $\mathbf{B}_{k-1|k-1}$  is composed of the value of  $f(\mathbf{X})$  and the first order reciprocal value.

$$\tilde{q}_{k-1|k-1}(\delta) = f(\mathbf{X}_{k-1|k-1}) + \nabla f(\mathbf{X}_{k-1|k-1})^T \delta + \frac{1}{2} \delta^T \mathbf{B}_{k-1|k-1} \delta \quad (6)$$

Use Eq. (6) to approach  $f(\mathbf{X})$ , and the minimum value of  $\tilde{q}_{k-1|k-1}(\delta)$  is regarded as the searching direction  $\mathbf{d}_{k-1|k-1}$ . The minimum value of  $\tilde{q}_{k-1|k-1}(\delta)$  is expressed as  $\delta = -\mathbf{B}_{k-1|k-1}^{-1} \nabla f(\mathbf{X}_{k-1|k-1})$ .

Assume

$$\mathbf{d}_{k-1|k-1} = -\mathbf{B}_{k-1|k-1}^{-1} \nabla f(\mathbf{X}_{k-1|k-1}) \quad (7)$$

The new iterative point is derived from:

$$\begin{aligned} \mathbf{X}'_{k|k-1} &= \mathbf{X}_{k-1|k-1} + \alpha_{k-1|k-1} \mathbf{d}_{k-1|k-1} \\ &= \mathbf{X}_{k-1|k-1} - \alpha_{k-1|k-1} \mathbf{B}_{k-1|k-1}^{-1} \nabla f(\mathbf{X}_{k-1|k-1}) \end{aligned} \quad (8)$$

where  $\alpha_{k-1|k-1}$  is determined through the linear search.

*Theorem 1:* Assume  $f(\mathbf{X})$  is the positive definite quadratic function, namely,  $f(\mathbf{X}) = \frac{1}{2} \mathbf{X}^T \mathbf{G} \mathbf{X} + \mathbf{p}^T \mathbf{X}$ , where  $\mathbf{G}$  is the positive matrix and  $\mathbf{p}$  is the  $n$  dimension vector, so Broyden's Quasi-Newton with accurate linear search has some characteristics as follows:

$$\mathbf{H}_{k+1} \mathbf{y}_i = \delta_i, \quad i = 0, 1, \dots, k \quad (9)$$

$$\delta_k^T \mathbf{G} \delta_i = 0, \quad i = 0, 1, \dots, k-1 \quad (10)$$

Not until  $m$ th ( $m \leq n$ ) iteration, does the whole loop terminate.

*Proof 1:* Because  $f(\mathbf{X})$  is the quadratic function, therefore,

$$\mathbf{y}_i = \mathbf{G} \delta_i \quad (11)$$

According to the accurate linear search,

$$\mathbf{g}_{i+1}^T \delta_i = 0 \quad (12)$$

When  $k = 0$ , according to the Quasi-Newton condition, therefore

$$\mathbf{H}_1 \mathbf{y}_0 = \delta_0 \quad (13)$$

Eq. (9) is tenable when  $k = 0$ .

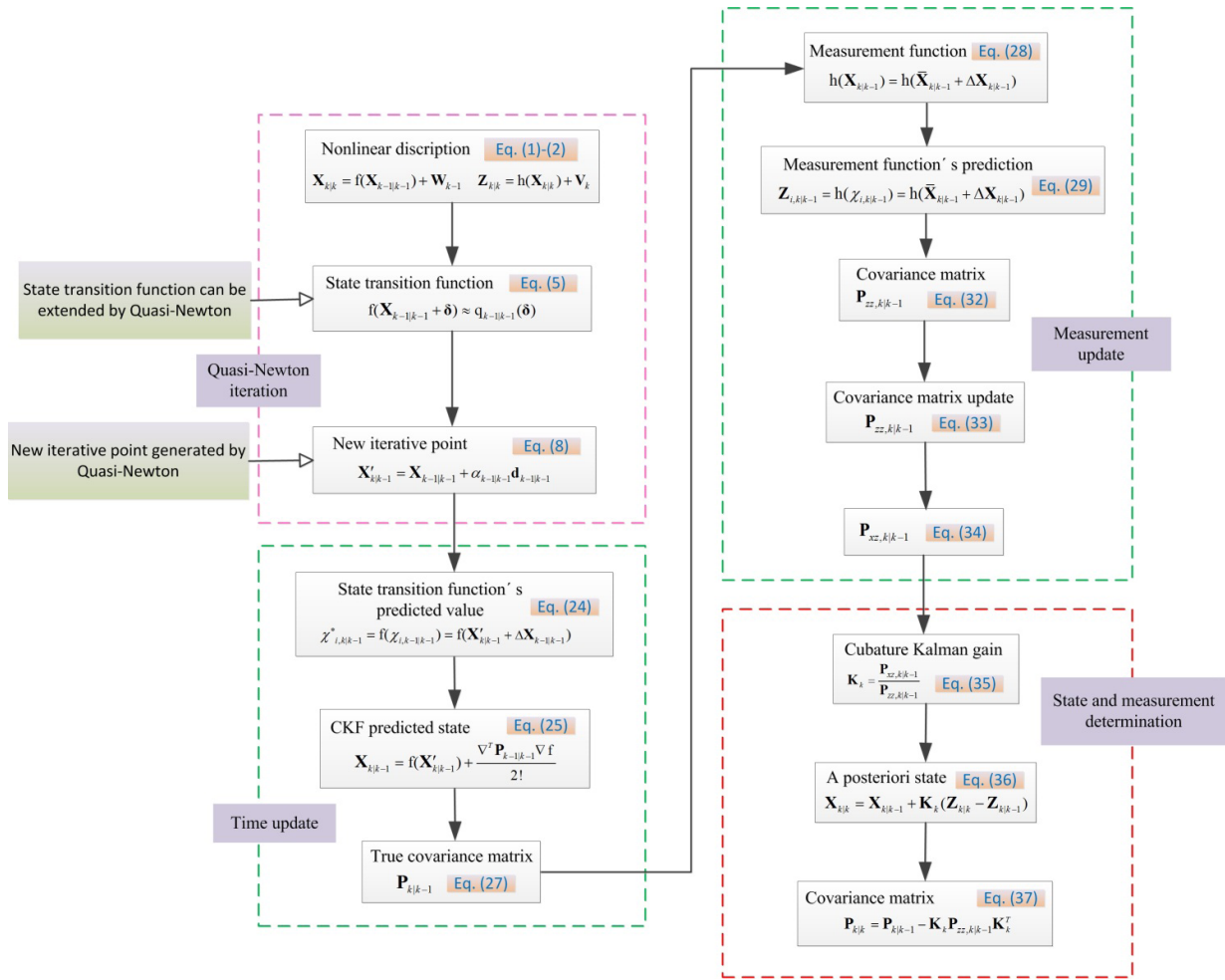


FIGURE 1. Flow diagram of QNCKF method.

When  $k = 1$ ,

$$\begin{aligned} \mathbf{g}_{i+1}^T \mathbf{G} \delta_0 &= (\mathbf{X}_2 - \mathbf{X}_1)^T \boldsymbol{\gamma}_0 = (-\alpha_1 \mathbf{H}_1 \mathbf{g}_1)^T \boldsymbol{\gamma}_0 \\ &= -\alpha_1 \mathbf{g}_1^T \mathbf{H}_1 \boldsymbol{\gamma}_0 = -\alpha_1 \mathbf{g}_1^T \delta_0 = 0 \end{aligned} \quad (14)$$

$\forall 0 \leq i \leq k$ , according to Eq. (11), Eq. (12) and Induction Hypothesis, then:

$$\begin{aligned} \mathbf{g}_{i+1}^T \mathbf{G} \delta_i &= -\alpha_{k+1} \mathbf{g}_{k+1}^T \mathbf{H}_{k+1} \boldsymbol{\gamma}_i = -\alpha_{k+1} \mathbf{g}_{k+1}^T \delta_i \\ &= \begin{cases} 0, & i = k \\ -\alpha_{k+1} \left[ \mathbf{g}_{i+1}^T \delta_i + \sum_{j=i+1}^k (\mathbf{g}_{j+1} - \mathbf{g}_j)^T \delta_i \right], & i \leq k-1 \end{cases} \\ &= \begin{cases} 0, & i = k \\ -\alpha_{k+1} \left[ 0 + \sum_{j=i+1}^k \delta_j^T \mathbf{G} \delta_i \right], & i \leq k-1 \end{cases} \\ &= 0 \end{aligned} \quad (15)$$

Therefore, it can derive:

$$\delta_{k+1}^T \mathbf{G} \delta_i = 0, \quad i = 0, 1, \dots, k \quad (16)$$

When  $i = k + 1$ , according to Quasi-Newton condition. Therefore,

$$\mathbf{H}_{k+2} \boldsymbol{\gamma}_{k+1} = \delta_{k+1} \quad (17)$$

When  $i \leq k$ ,

$$\begin{aligned} \mathbf{H}_{k+2} \boldsymbol{\gamma}_i &= \mathbf{H}_{k+1} \boldsymbol{\gamma}_i + \frac{\delta_{k+1} \delta_{k+1}^T \boldsymbol{\gamma}_i}{\delta_{k+1}^T \boldsymbol{\gamma}_{k+1}} \\ &\quad - \frac{\mathbf{H}_{k+1} \boldsymbol{\gamma}_{k+1} \boldsymbol{\gamma}_{k+1}^T \mathbf{H}_{k+1} \boldsymbol{\gamma}_i}{\boldsymbol{\gamma}_{k+1}^T \mathbf{H}_{k+1} \boldsymbol{\gamma}_{k+1}} + \phi \mathbf{v}_{k+1} \mathbf{v}_{k+1}^T \boldsymbol{\gamma}_i \end{aligned} \quad (18)$$

Based on Eq. (11), Eq. (16) and Induction Hypothesis, it can derive:

$$\delta_{k+1}^T \boldsymbol{\gamma}_i = \delta_{k+1}^T \mathbf{G} \delta_i = 0 \quad (19)$$

$$\boldsymbol{\gamma}_{k+1}^T \mathbf{H}_{k+1} \boldsymbol{\gamma}_i = \boldsymbol{\gamma}_{k+1}^T \delta_i = \delta_{k+1}^T \mathbf{G} \delta_i = 0 \quad (20)$$

$$\begin{aligned} \mathbf{v}_{k+1}^T \boldsymbol{\gamma}_i &= (\boldsymbol{\gamma}_{k+1}^T \mathbf{H}_{k+1} \boldsymbol{\gamma}_{k+1})^{\frac{1}{2}} \\ &\quad \times \left( \frac{\delta_{k+1}^T}{\delta_{k+1}^T \boldsymbol{\gamma}_{k+1}} - \frac{\boldsymbol{\gamma}_{k+1}^T \mathbf{H}_{k+1}}{\boldsymbol{\gamma}_{k+1}^T \mathbf{H}_{k+1} \boldsymbol{\gamma}_{k+1}} \right) \boldsymbol{\gamma}_i = 0 \end{aligned} \quad (21)$$



Therefore,

$$\mathbf{H}_{k+2}\boldsymbol{\gamma}_i = \mathbf{H}_{k+1}\boldsymbol{\gamma}_i = \boldsymbol{\delta}_i, \quad i = 0, 1, \dots, k + 1 \quad (22)$$

Eq. (9) and Eq. (10) are proved.

Because  $\boldsymbol{\delta}_i$  ( $i = 0, 1, \dots, n - 1$ ) is conjugate for  $\mathbf{G}$ , according to Conjugate Direction Principle, Broyden's class of Quasi-Newton methodology does will stop no more than  $n$ th step.

*Theorem 2:* Assume  $\mathbf{X}_0$  is a random initial point,  $f(\mathbf{X})$  is second-order continuously differentiable and is uniformly convex in the level set  $L(\mathbf{X}_0) = \{\mathbf{X}|f(\mathbf{X}) \leq f(\mathbf{X}_0)\}$ , so there exists  $m > 0$  to satisfy:

$$\mathbf{u}^T \nabla^2 f(\mathbf{X}) \mathbf{u} \geq m \|\mathbf{u}\|^2, \quad \forall \mathbf{u} \in \mathbf{R}^n, \quad \mathbf{X} \in L(\mathbf{X}_0) \quad (23)$$

For any a positive definite matrix  $\mathbf{H}_0$ , the step length factor  $\alpha_k$  is determined by:

- (a) Accurate linear search;
- (b) Wolfe-Powell Criterion;

So the point column  $\{\mathbf{X}_k\}$  produced by Broyden's class of Quasi-Newton methodology converges to the minimum of  $f(\mathbf{X})$ .

## 2) STATE ESTIMATE UPDATE

Use the first predicted value  $\mathbf{X}'_{k|k-1}$  to update Cubature points  $\chi_{i,k-1|k-1} = \mathbf{X}'_{k|k-1} + \sqrt{n\mathbf{P}_{k-1|k-1}}$ , and then the state transition function's predicted value of each Cubature point is:

$$\begin{aligned} \chi_{i,k|k-1}^* &= f(\chi_{i,k-1|k-1}) = f(\mathbf{X}'_{k|k-1} + \Delta\mathbf{X}_{k-1|k-1}) \\ &= f(\mathbf{X}'_{k|k-1}) + D_{\Delta\mathbf{X}_{k-1|k-1}}f + \frac{D_{\Delta\mathbf{X}_{k-1|k-1}}^2 f}{2!} \\ &\quad + \frac{D_{\Delta\mathbf{X}_{k-1|k-1}}^3 f}{3!} + \frac{D_{\Delta\mathbf{X}_{k-1|k-1}}^4 f}{4!} + \dots \quad (24) \end{aligned}$$

Because  $\Delta\mathbf{X}_{k|k-1}$  is symmetrically distributed, all the odd moments sum up to zero. Moreover, keep the second order term by neglecting higher order terms to simply complex calculation. The second predicted value  $\mathbf{X}_{k|k-1}$  is:

$$\mathbf{X}_{k|k-1} = f(\mathbf{X}'_{k|k-1}) + \frac{\nabla^T \mathbf{P}_{k-1|k-1} \nabla f}{2!} \quad (25)$$

As the terms higher than three are neglected,  $\chi_{i,k-1|k-1}^* - \mathbf{X}_{k|k-1}$  can be determined as follows:

$$\begin{aligned} \chi_{i,k-1|k-1}^* - \mathbf{X}_{k|k-1} &= D_{\Delta\mathbf{X}_{k|k-1}}f + \frac{D_{\Delta\mathbf{X}_{k|k-1}}^2 f}{2!} \\ &\quad + \frac{D_{\Delta\mathbf{X}_{k|k-1}}^3 f}{3!} - E \left[ \frac{D_{\Delta\mathbf{X}_{k|k-1}}^2 f}{2!} \right] \quad (26) \end{aligned}$$

Because of the symmetry of  $\Delta\mathbf{X}_{k|k-1}$ , the mean value of all odd order terms of  $\Delta\mathbf{X}_{k|k-1}$  is equal to zero, and the true

covariance matrix is expressed as:

$$\begin{aligned} \mathbf{P}_{k|k-1} &= \Phi_k \mathbf{P}_{k-1|k-1} \Phi_k^T + E \left[ \begin{aligned} &\frac{D_{\Delta\mathbf{X}_{k-1|k-1}} f (D_{\Delta\mathbf{X}_{k-1|k-1}}^3 f)^T}{3!} + \\ &\frac{D_{\Delta\mathbf{X}_{k-1|k-1}}^2 f (D_{\Delta\mathbf{X}_{k-1|k-1}}^2 f)^T}{2 \times 2!} + \\ &\frac{D_{\Delta\mathbf{X}_{k-1|k-1}}^3 f (D_{\Delta\mathbf{X}_{k-1|k-1}} f)^T}{3!} \end{aligned} \right] \\ &\quad - \left[ \left( \frac{\nabla^T \mathbf{P}_{k-1|k-1} \nabla}{2!} \right) f \right] \left[ \left( \frac{\nabla^T \mathbf{P}_{k-1|k-1} \nabla}{2!} \right) f \right]^T + \mathbf{Q}_k \quad (27) \end{aligned}$$

where  $\Phi_k$  is the Jacobian matrix of  $f(\cdot)$ ;  $D_{\Delta\mathbf{X}}f = \left[ (\Delta\mathbf{X}^T \nabla) f(\chi) \right]^T \Big|_{\mathbf{X}=\bar{\mathbf{X}}}$ ;  $\nabla$  denotes the differential of  $f(\mathbf{X})$ ;

It shows from Eq. (25) and Eq. (27) that QNCKF can seize and multiply the second order terms of a nonlinear system. But in a linear or linearized system, more than second order terms are zero. Thus, Eq. (25) and Eq. (27) will be same as EKF.

Consider the random variable  $\mathbf{X}_{k|k-1}$  with mean  $\bar{\mathbf{X}}_{k|k-1}$  and covariance matrix  $\mathbf{P}_{k|k-1}$  of Gaussian distribution  $\mathbf{X}_{k|k-1} \sim N(\bar{\mathbf{X}}_{k|k-1}, \mathbf{P}_{k|k-1})$ . Define  $\Delta\mathbf{X}_{k|k-1}$  as  $\mathbf{X}_{k|k-1} - \bar{\mathbf{X}}_{k|k-1}$  with Gaussian distribution  $\Delta\mathbf{X}_{k|k-1} \sim N(0, \mathbf{P}_{k|k-1})$  as described in the above analysis. The measurement function  $h(\mathbf{X}_{k|k-1})$  could be extended into a Taylor series around  $\bar{\mathbf{X}}_{k|k-1}$  as:

$$\begin{aligned} h(\mathbf{X}_{k|k-1}) &= h(\bar{\mathbf{X}}_{k|k-1} + \Delta\mathbf{X}_{k|k-1}) \\ &= h(\bar{\mathbf{X}}_{k|k-1}) + D_{\Delta\mathbf{X}_{k|k-1}}h + \frac{D_{\Delta\mathbf{X}_{k|k-1}}^2 h}{2!} \\ &\quad + \frac{D_{\Delta\mathbf{X}_{k|k-1}}^3 h}{3!} + \frac{D_{\Delta\mathbf{X}_{k|k-1}}^4 h}{4!} + \dots \quad (28) \end{aligned}$$

Substitute the Cubature points  $\chi_{i,k|k-1} = \bar{\mathbf{X}}_{k|k-1} + \sqrt{n\mathbf{P}_{k|k-1}}$  into Eq. (28), and the measurement function's prediction of each Cubature point is written as:

$$\begin{aligned} \mathbf{z}_{i,k|k-1} &= h(\chi_{i,k|k-1}) = h(\bar{\mathbf{X}}_{k|k-1} + \Delta\mathbf{X}_{k|k-1}) \\ &= h(\bar{\mathbf{X}}_{k|k-1}) + D_{\Delta\mathbf{X}_{k|k-1}}h + \frac{D_{\Delta\mathbf{X}_{k|k-1}}^2 h}{2!} \\ &\quad + \frac{D_{\Delta\mathbf{X}_{k|k-1}}^3 h}{3!} + \frac{D_{\Delta\mathbf{X}_{k|k-1}}^4 h}{4!} + \dots \quad (29) \end{aligned}$$

Like the computation in the prediction value of state transition function, the mean value of measurement Cubature points is derived by neglecting the higher order terms:

$$\mathbf{z}'_{k|k-1} = h(\bar{\mathbf{X}}_{k|k-1}) + \frac{\nabla^T \mathbf{P}_{k|k-1} \nabla h}{2!} \quad (30)$$

$\mathbf{z}_{k|k-1} - \mathbf{z}'_{k|k-1}$  can be determined by:

$$\begin{aligned} \mathbf{z}_{k|k-1} - \mathbf{z}'_{k|k-1} &= D_{\Delta\mathbf{X}_{k|k-1}}h + \frac{D_{\Delta\mathbf{X}_{k|k-1}}^2 h}{2!} \\ &\quad + \frac{D_{\Delta\mathbf{X}_{k|k-1}}^3 h}{3!} - E \left[ \frac{D_{\Delta\mathbf{X}_{k|k-1}}^2 h}{2!} \right] \quad (31) \end{aligned}$$

$\mathbf{P}_{zz,k|k-1}$  is expressed as:

$$\mathbf{P}_{zz,k|k-1} = E[(\mathbf{Z}_{k|k-1} - \mathbf{Z}'_{k|k-1})(\mathbf{Z}_{k|k-1} - \mathbf{Z}'_{k|k-1})^T] + \mathbf{R}_k \quad (32)$$

Making use of the symmetry of  $\Delta\mathbf{X}_{k|k-1}$ , the mean value of all odd order terms of  $\Delta\mathbf{X}_{k|k-1}$  is equal to zero and the covariance matrix is updated again:

$$\begin{aligned} \mathbf{P}_{zz,k|k-1} &= \mathbf{H}_k \mathbf{P}_{k|k-1} \mathbf{H}_k^T + E \left[ \begin{array}{c} D_{\Delta\mathbf{X}_{k|k-1}} h (D_{\Delta\mathbf{X}_{k|k-1}}^3 h)^T \\ + \frac{D_{\Delta\mathbf{X}_{k|k-1}}^2 h (D_{\Delta\mathbf{X}_{k|k-1}}^2 h)^T}{2 \times 2!} \\ + \frac{D_{\Delta\mathbf{X}_{k|k-1}}^3 h (D_{\Delta\mathbf{X}_{k|k-1}} h)^T}{3!} \end{array} \right] \\ &\quad - E \left[ \frac{\nabla^T \mathbf{P}_{k|k-1} \nabla}{2!} h \right] E \left[ \frac{\nabla^T \mathbf{P}_{k|k-1} \nabla}{2!} h \right]^T + \mathbf{R}_k \quad (33) \end{aligned}$$

By definition,  $\mathbf{P}_{xz,k|k-1}$  is written as follows:

$$\mathbf{P}_{xz,k|k-1} = \mathbf{P}_{k|k-1} \mathbf{H}_k^T + E \left[ \Delta\mathbf{X}_{k|k-1} \frac{D^3 \Delta\mathbf{X}_{k|k-1} h}{3!} \right]^T \quad (34)$$

Then the Cubature Kalman gain is derived from:

$$\mathbf{K}_k = \frac{\mathbf{P}_{xz,k|k-1}}{\mathbf{P}_{zz,k|k-1}} \quad (35)$$

The posteriori state and the covariance matrix are given as follows, respectively:

$$\mathbf{X}_{k|k} = \mathbf{X}_{k|k-1} + \mathbf{K}_k (\mathbf{Z}_{k|k} - \mathbf{Z}_{k|k-1}) \quad (36)$$

$$\mathbf{P}_{k|k} = \mathbf{P}_{k|k-1} - \mathbf{K}_k \mathbf{P}_{zz,k|k-1} \mathbf{K}_k^T \quad (37)$$

It is concluded from the analysis of QNCKF estimation accuracy that QNCKF is not only related to the first order terms but also the second order terms of the covariance matrix, indicating the ability of QNCKF to seize higher order terms of nonlinear functions. Nevertheless, if the system is linear or the non-linearity of the system is not very high, the higher order terms are deemed to be zero and QNCKF performs as well as EKF.

### III. EXPERIMENTS AND RESULTS

In order to verify the performance of the proposed algorithm, the real tests in a boat and a glider are carried out using the new underwater inertial navigation system which is designed in our lab (Model number: SUNS), as shown in Table 1. This system is made up of a digital signal processing (DSP) unit and IMU which mainly includes tri-axis MEMS angular rate sensors, tri-axis MEMS acceleration sensors and tri-axis magnetic sensors. The size of SUNS is 0.385dm<sup>3</sup> and the power consumption is less than 0.6W. The raw information from IMU is processed through signal conditioning and conversion. The calibrated data is fed back into the multi-sensor data fusion module. The updated navigation information is transmitted through the serial port. When the glider dives underwater, the navigation information is acquired by the inertial navigation system. Before the glider dives into the

TABLE 1. The specifications for the test system (SUNS).

Physical Characteristics	
Length (m)	0.11
Width (m)	0.07
Height (m)	0.05
Weight (g)	<250
Power (W)	<0.6





TABLE 2. The specifications for the reference system (GNSS system).

Physical Characteristics	
Output rate (Hz)	200
Gyro rate bias (deg/hr)	< 1.0
Gyro scale factor (ppm)	100
Angular random walk (deg/sqrt(hr))	< 0.05
Accelerometer scale factor (ppm)	250
Accelerometer bias (mg)	< 1.0



lake or after it floats out the lake surface, the glider will obtain the precise position information via GPS. Moreover, other devices are together carried on the boat and the glider to set up an effective test platform using the method proposed in this paper.

#### A. EVALUATION OF ALGORITHM

The glider usually follows a sawtooth motion pattern in the vertical plane and progresses along a straight line or several piecewise lines in the horizontal plane [50]. The change of depth is measured by the depthometer or other instruments, and it may be not the focus in this paper. The acquisition of navigation information mainly by the inertial system in the horizontal plane is studied here. In order to verify the performance of the proposed method in the underwater processing of gliding, the boat experiments are performed along a trajectory as complex as possible. The boat experiments were done in the Mahe Reservoir, China. The experiments were conducted on a boat platform mainly equipped with SUNS and NovAtel GNSS Inertial System (hereinafter referred to as GNSS system). This GNSS system integrates UIMU-LCI tactical grade IMU with a NovAtel OEM6 GPS receiver in a tightly coupled fashion, and uses the world-leading GNSS+INS SPAN technology. Therefore, it provides the high-end reference to validate the performance of proposed method here, which currently works in a loosely coupled mode. The specifications for GNSS system are shown in Table 2. SUNS and GNSS system are all fixed on the same plane. The initial attitude angles (heading, pitch and roll) differences between two devices are recorded and can be compensated in the later signal processing.

#### 1) EXPERIMENTS WITHOUT MAGNETIC INTERFERENCE

The boat trajectory obtained by GNSS System is shown in Fig. 2(a). The velocities in the east direction and north

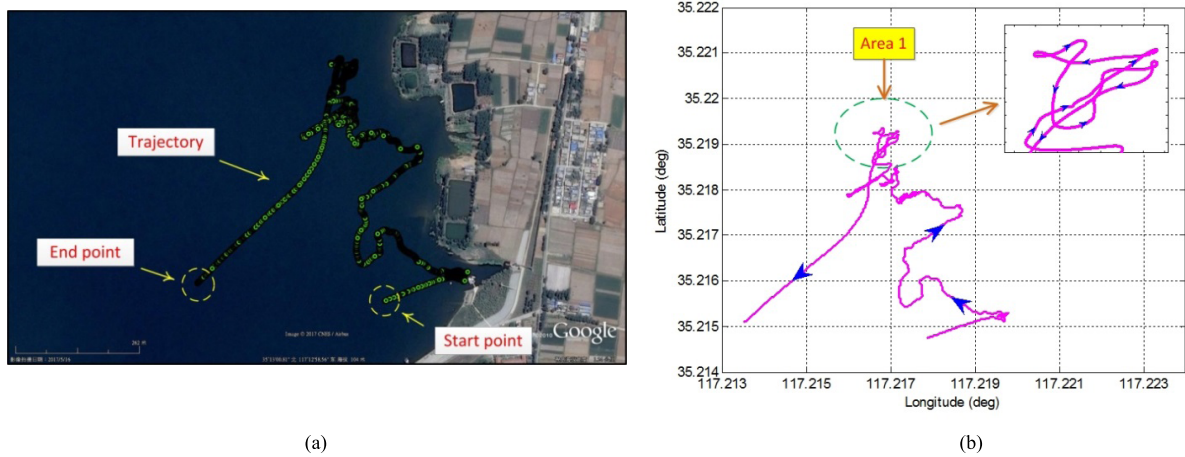


FIGURE 2. (a) Map of the running trajectory, (b) coordinates of the running trajectory and Area 1.

TABLE 3. Errors comparison of different algorithms for the entire path and the local path.

	RMSE					
	EKF		CKF		QNCKF	
	Entire path	Local path (Area 1)	Entire path	Local path (Area 1)	Entire path	Local path (Area 1)
Heading (deg)	0.8937	0.8511	0.8623	0.8437	0.8201	0.8301
Pitch (deg)	0.2797	0.2716	0.2253	0.2372	0.2209	0.2187
Roll (deg)	0.2195	0.2240	0.2206	0.2135	0.2022	0.2115

direction are shown in Fig. 3 and Fig. 4, respectively. The root mean square errors (RMSE) of attitudes for EKF, CKF and QNCKF are shown in Table 3. It can be seen from Figs. 3-4 that the velocities of boat in east and north are similar as velocities of glider during gliding underwater (about 0.25m/s-1m/s gliding velocity for a glider) [18]. Therefore, the boat experiment results can verify the performance of algorithms applied to glider to the most extent. In Table 3, it is concluded that QNCKF, CKF and EKF show quite a similar performance for heading angle, pitch angle and roll angle because heading angle, pitch angle and roll angle are observable in the experiment area. The accuracy similarity among three methods indicates the observability has an effect on the performance of filtering method.

In order to evaluate the performance of proposed algorithm for the estimation of attitude especially in the larger change of angle, the boat goes along routes as complex as possible. As is shown in Area 1 in Fig. 2(b), the boat trajectory includes a number of turning processes, and some accelerating or decelerating cases. The attitude comparisons between EKF, CKF and QNCKF in the turning case are shown in Figs. 5-7 and the RMSE of attitudes for three algorithms are also shown in Table 3. In Table 3, we can clearly compare that, it nearly has no difference between usual trajectories and complex trajectories for the estimation accuracy of different algorithms.

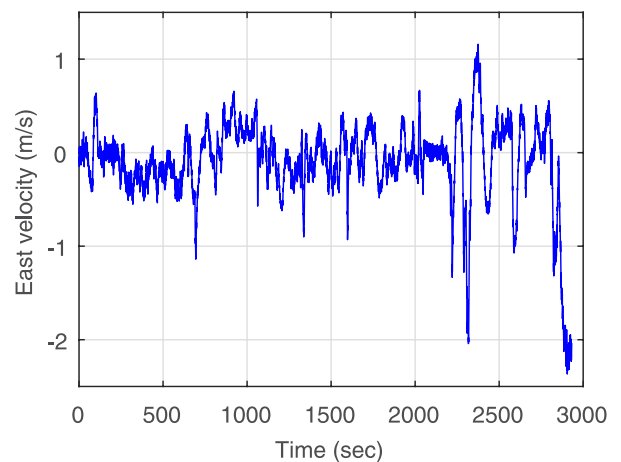


FIGURE 3. East velocity of boat.

It also suggests that the performances of different algorithms (EKF, CKF and QNCKF) are not influenced during the much larger change of heading angle.

QNCKF, CKF and EKF have similar heading, pitch and roll estimation accuracy because all angle components are observable. The measurements have the capability in restraining estimation error accumulation and scaling down the non-linearity of the system. The linear psi-angle expression is usually valid, and there is a remarkable resemblance between

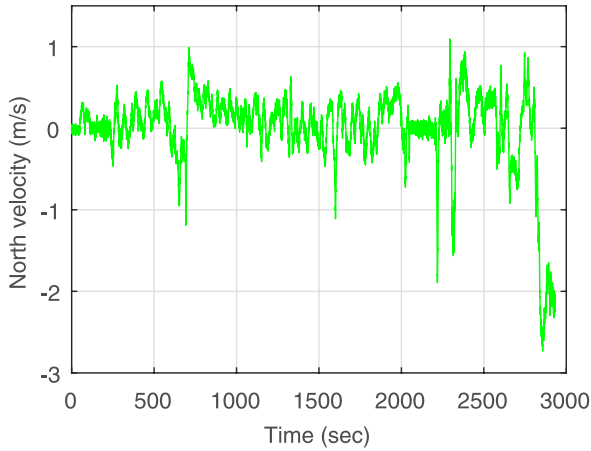


FIGURE 4. North velocity of boat.

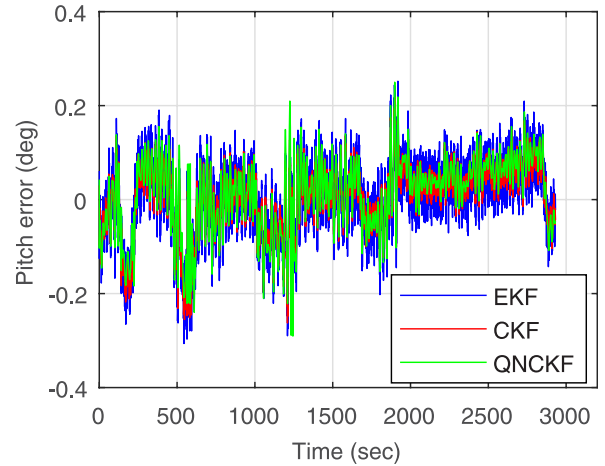


FIGURE 6. Pitch errors for different algorithms.

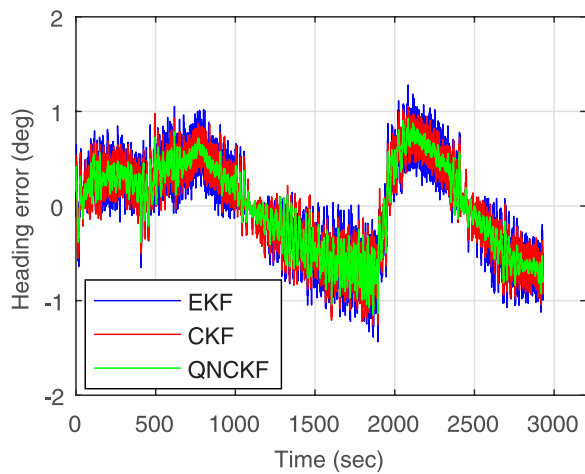


FIGURE 5. Heading errors for different algorithms.

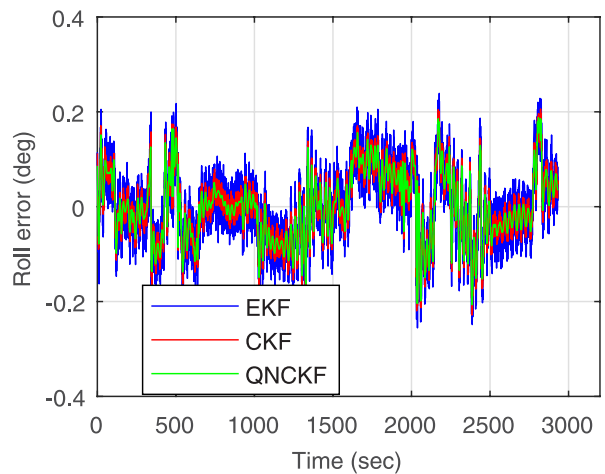


FIGURE 7. Roll errors for different algorithms.

the nonlinear attitude expression and the linear psi-angle expression. Considering analysis in CKF and QNCKF estimation accuracy, it will not be productive to employ QNCKF and CKF in a linear system. Thus, QNCKF and CKF do not show higher accuracy than EKF in the observable cases.

However, as shown in Fig. 8, the computation time of CKF is 1822.85ms, while the computation time of QNCKF and EKF is 211.53ms and 190.57ms, respectively. QNCKF and EKF has far lower computational burden than CKF. Therefore, although CKF has the similar estimation accuracy in the measurement observation case, the computation efficiency of CKF is much lower than two others.

2) EXPERIMENTS WITH MAGNETIC INTERFERENCE

During the coasting period, the magnetic sensor is interfered artificially from 1250s to 1850s, and the navigation system is switched to only both gyroscopes and accelerometers. Because there is no aiding sensor to correct heading information calculated by gyroscopes, the estimation errors accumulate rather fast, resulting in heading estimation inaccurate. Fig. 9 show the heading error comparison results between the proposed QNCKF and other algorithms.

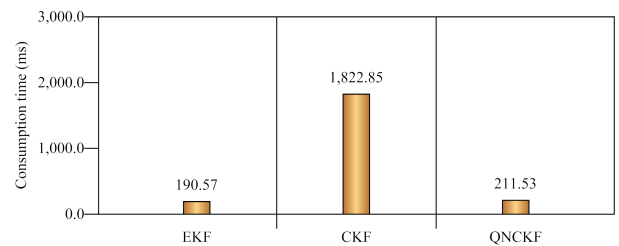


FIGURE 8. Computational load comparison for different algorithms.

Furthermore, the RMSE of attitudes for EKF, CKF and QNCKF are shown in Table 4. It is clearly seen from Fig. 9 that by employing EKF, the maximum of heading increases from  $0.2625^\circ$  to  $1.05^\circ$ , and the minimum slumps from  $-0.375^\circ$  to  $-1.025^\circ$ . However, QNCKF and CKF do not nearly suffer from the interference, and they will still provide stable and accurate heading information. During the interference period, the observations are unavailable, so the states could accordingly be regarded as unobservable, which causes the estimation errors to accumulate very fast. The nonlinear



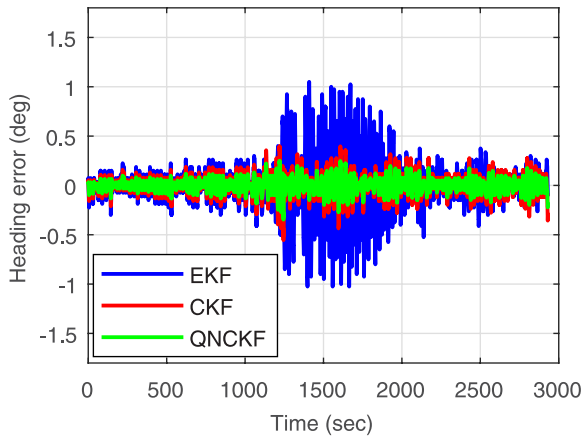


FIGURE 9. Heading error when magnetic sensors are interfered.

TABLE 4. Comparison of errors for EKF, CKF and QNCKF.

	RMSE		
	EKF	CKF	QNCKF
Heading (deg)	0.9808	0.3935	0.3514

attitude expression employed in CKF and QNCKF can restraint the attitude error accumulation because of their high model prediction accuracy.

From the attitude comparison among QNCKF, CKF and EKF in the scenario with interference, it indicates that the heading angle accuracy is improved by employing QNCKF and CKF in the unobservable cases, but the accuracy of state estimation is influenced slightly in observation cases where the heading accuracy is mainly determined by the model prediction accuracy. QNCKF and CKF have higher estimation accuracy than EKF in the unobservable case and it can be interpreted from two aspects. On the one hand, when the heading error accumulates rather fast and becomes quite large, the linear traditional psi-angle expression will become unavailable while the nonlinear attitude expression still performs better. The traditional attitude error expression is less accurate than the nonlinear one. On the other hand, as shown by the Taylor analysis in the QNCKF and CKF prediction, one can see that QNCKF and CKF would seize higher-order terms of the nonlinear function, but the higher order terms are ignored for EKF. Different from QNCKF and CKF, EKF cannot seize the higher-order terms when it is implemented with nonlinear attitude error expression for state determination. Thanks to the higher prediction accuracy of QNCKF and CKF, they have lower heading drifts than EKF in the nonlinear cases.

As concluded by the observability analysis, the heading angle’s degree of observability changes in the different scenarios. The lower the observability, the more obvious superiority of QNCKF and CKF are. For instance, during the period of magnetic interference, the heading angle accuracy

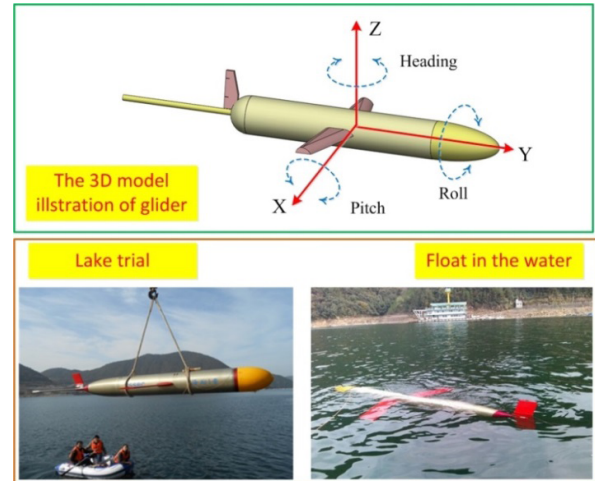


FIGURE 10. The glider in the lake trial.

improves much obviously by using QNCKF and CKF. On the contrary, the improvement is rather small in the non-inference case, and the estimation accuracy of QNCKF and CKF are nearly the same as one of EKF in all the observable cases. As the pitch angle and roll angle are always observable, thus they have nearly equal prediction accuracy in the experiments.

The application of EKF only minimizes the consumption of time in deriving the Jacobian matrix. EKF outperforms CKF in terms of computational load. The nonlinear attitude error expression includes a few cosine and sine calculations. The nonlinear state transition function will be implemented  $2n$  times in one CKF filtering cycles. Therefore, CKF consumes much more time than EKF. Beyond that, as shown in CKF, the generation of cubature points demands a matrix decomposition calculation. The singular value matrix decomposition method not only is robust but also requires plenty of computational time. Thus, the computational burden of CKF is higher than one of EKF. QNCKF makes better use of the advantages of CKF and EKF to provide high accuracy estimations efficiently.

**B. EVALUATION OF ALGORITHM APPLIED TO A GLIDER**

The complex underwater environment causes larger errors for MEMS inertial sensors and makes the nonlinear degree of model higher. Moreover, magnetic sensors are also influenced by the inevitable and sudden magnetic interference such as surrounding boats with coming and going, sudden electromagnetic interference from outside and so on. In such a case, the measurement of magnetic becomes inaccurate even erroneous. The states become unobservable and it is hard to obtain the accurate estimations of attitudes. The performance of proposed method is evaluated through the real underwater glider experiments. The navigation platform consists of “Haixiang” glider and other sensors carried in the glider. Data related to angular rate, acceleration and attitudes of the glider are measured by SUNS which is



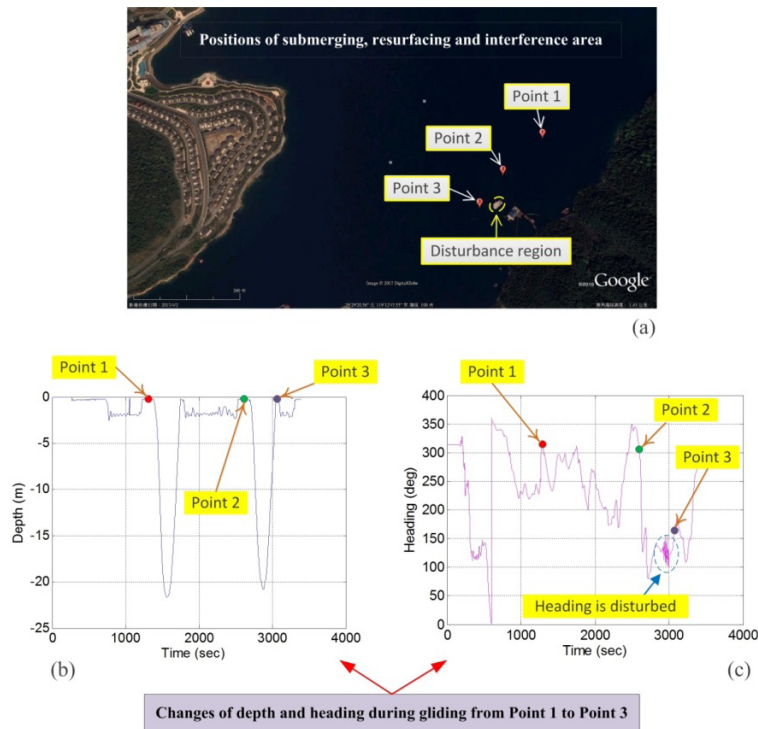


**FIGURE 11.** Position of glider, changes of depth and heading during gliding from Point 1 to Point 3.

loaded in the glider. The SUNS is installed in the center of glider to move away from some interference resources in the glider. The velocity of glider can also be calculated by accelerometers, and at the same time estimated by DR module. The attitudes (heading, pitch and roll) can also be acquired by INS aided with magnetic sensors.

This glider is tested in Thousand Island Lake, China, as shown in Fig. 10. Trials are performed at a speed of glider between 0.35 m/s and 0.65 m/s. In Fig. 11(a), Point 1 (Latitude: 29° 29'22.29" N; Longitude: 119° 13'3.91" E) represents the initial position of diving; Point 2 (Latitude: 29° 29' 18.77"N; Longitude: 119° 12' 59.49" E) devotes the position of first rising to the surface; Point 3 (Latitude: 29° 29' 15.71" N; Longitude: 119° 12' 56.89" E) is the second resurfacing position. The yellow box area in Fig. 11(a) indicates the interference area where a barge is moored. The changes of depth and heading angle are also shown in Fig. 11(b)-(c). The errors of heading by using different algorithms in the period from Point 1 to Point 3 are shown in Table 5. In the lake trial, the glider acquires a number of raw data, and the satisfactory results are achieved.

As shown in Fig. 11(b), the glider is rising from 2913s to 3020s and gradually approach to the barge so that magnetic sensors are disturbed. The heading angle is interfered between Point 2 and Point 3, shown in Fig. 11(c), and the glider is gliding near the barge which causes more magnetic interferences, thus the measurement errors of magnetic sensors are increased. Fig. 12 shows heading errors for different

**TABLE 5.** Comparison of errors for EKF, CKF and QNCKF.

	RMSE		
	EKF	CKF	QNCKF
Heading (deg)	1.2576	0.3844	0.3336

algorithms during gliding and the comparison results are presented in Table 5.

It is seen from Fig. 12 and Table 5 that QNCKF, CKF and EKF have similar measurement accuracies in the non-interference because the measurements are observable. When the magnetic sensors are disturbed from the outside environment and the measurements are unobservable, the errors of EKF become obviously larger. However, QNCKF and CKF still maintain the stable accuracy in the attitude estimation, reflecting their better advantages than EKF in interference scenarios.

The experiment area includes the interference area and the non-interference area. If the states become fully observable in some particular cases, it is difficult to confirm that nonlinear filtering methods (CKF and QNCKF) must outweigh EKF. QNCKF and CKF can seize and multiply the second order terms of a non-linear system, but when they are used in a linear or linearized system, the higher-order terms containing second-order terms are zero. When the magnetic sensors are disturbed and the measurements become unobservable,

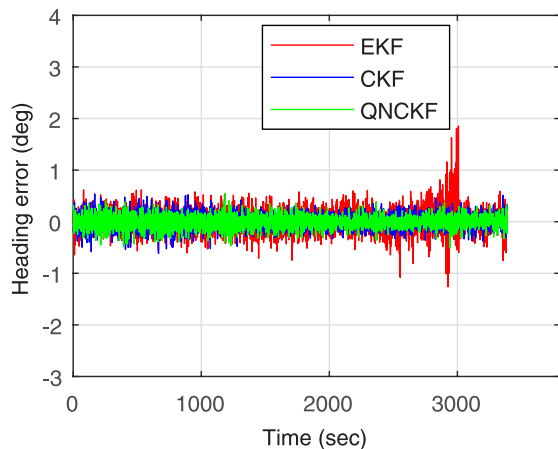


**FIGURE 12.** Heading error for different algorithms during gliding from Point 1 to Point 3.

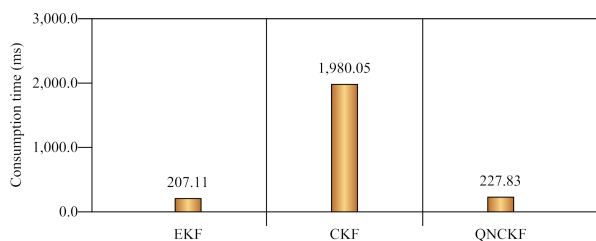


**FIGURE 13.** Computational load comparison for different algorithms.

the heading angle estimation accuracy is usually a difficult task for EKF because the measurements do not exert any effect on heading prediction. The unobservability will bring about a fast accumulation of prediction errors and make the linear expression unavailable. In such a scenario, the performances of QNCKF and CKF in terms of heading estimation are outstanding. Since the pitch and roll angles are observable during the whole gliding, their accuracies are not degraded for different algorithms. However, the major difference between QNCKF and CKF is that CKF has much larger computational load than QNCKF, as shown in Fig. 13. The QNCKF, fully absorbing the advantages of Quasi-Newton method and the CKF, can perform better in aspect of accuracy and computational efficiency.

#### IV. CONCLUSION

In this paper, the performances of different algorithms are verified in an INS aided with a magnetic sensor based on both mathematical deductions and experiments. The prediction accuracies of QNCKF and CKF are validated through a Taylor expansion. It is proved that QNCKF and CKF have a similar estimation precision as EKF when employed in linear or linearized systems. On the basis of the above conclusion, a nonlinear attitude description is introduced into the navigation system to demonstrate the merits of CKF and QNCKF. The observability of the heading angle changes under disparate scenarios. Therefore, the performances of QNCKF and CKF under different maneuvers are further evaluated on the

basis of observability analysis. One can conclude from the experimental results that QNCKF and CKF outperform EKF, especially when low-cost MEMS sensors are interfered to cause the measurements unobservable or lower observable, but the computational load of CKF is far higher than others. Therefore, QNCKF has the highest priority in terms of estimation accuracy and computation efficiency among three methods.

#### REFERENCES

- [1] C. C. Eriksen *et al.*, “Seaglider: A long-range autonomous underwater vehicle for oceanographic research,” *IEEE J. Ocean. Eng.*, vol. 26, no. 4, pp. 424–436, Oct. 2001.
- [2] S. A. Jenkins and G. D’Spain, “Autonomous underwater glider,” in *Springer Handbook of Ocean Engineering*. Cham, Switzerland: Springer, 2016, pp. 301–321.
- [3] C. Jones, B. Allsup, and C. DeCollibus, “Slocum glider: Expanding our understanding of the oceans,” in *Proc. Oceans-St. John’s*, Sep. 2014, pp. 14–19.
- [4] J. Austin, “The potential for Autonomous Underwater Gliders in large lake research,” *J. Great Lakes Res.*, vol. 39, pp. 8–13, Jan. 2013.
- [5] D. C. Webb, P. J. Simonetti, and C. P. Jones, “SLOCUM: An underwater glider propelled by environmental energy,” *IEEE J. Ocean. Eng.*, vol. 26, no. 4, pp. 447–452, Oct. 2001.
- [6] J. Kim, Y. Park, S. Lee, and Y. K. Lee, “Underwater glider navigation error compensation using sea current data,” *IFAC Proceedings Volumes*, vol. 47, no. 3, pp. 9661–9666, 2014.
- [7] H. Kaushal and G. Kaddoum, “Underwater optical wireless communication,” *IEEE Access*, vol. 4, pp. 1518–1547, 2016.
- [8] D. L. Rudnick, C. C. Eriksen, D. M. Fratantoni, and M. J. Perry, “Underwater gliders for ocean research,” *Marine Technol. Soc. J.*, vol. 38, no. 2, pp. 74–84, 2004.
- [9] J. Sherman, R. E. Davis, W. B. Owens, and J. Valdes, “The autonomous underwater glider ‘Spray,’” *IEEE J. Ocean. Eng.*, vol. 26, no. 4, pp. 437–446, Oct. 2001.
- [10] H. Yang, W. Li, C. Luo, J. Zhang, and Z. Si, “Research on error compensation property of strapdown inertial navigation system using dynamic model of shearer,” *IEEE Access*, vol. 4, pp. 2045–2055, 2016.
- [11] H. Cao, H. Li, J. Liu, Y. Shi, J. Tang, and C. Shen, “An improved interface and noise analysis of a turning fork microgyroscope structure,” *Mech. Syst. Signal Process.*, vols. 70–71, pp. 1209–1220, Mar. 2016.
- [12] S. Chong *et al.*, “Temperature drift modeling of MEMS gyroscope based on genetic-Elman neural network,” *Mech. Syst. Signal Process.*, vols. 72–73, pp. 897–905, May 2016.
- [13] H. Nourmohammadi and J. Keighobadi, “Fuzzy adaptive integration scheme for low-cost SINS/GPS navigation system,” *Mech. Syst. Signal Process.*, vol. 99, pp. 434–449, Jan. 2018.
- [14] J. Zhang, Y. Su, Q. Shi, and A.-P. Qiu, “Microelectromechanical resonant accelerometer Designed with a high sensitivity,” *Sensors*, vol. 15, no. 12, pp. 30293–30310, Dec. 2015.
- [15] Y. Xu, X. Zhu, and Y. Su, “A novel network calibration method for inertial measurement units,” *Proc. Inst. Mech. Eng. G, J. Aerosp. Eng.*, vol. 229, no. 7, pp. 1336–1348, Jun. 2015.
- [16] J. Melo and A. Matos, “Survey on advances on terrain based navigation for autonomous underwater vehicles,” *Ocean Eng.*, vol. 139, pp. 250–264, Jul. 2017.
- [17] Z. Sun, X. Mao, W. Tian, and X. Zhang, “Activity classification and dead reckoning for pedestrian navigation with wearable sensors,” *Meas. Sci. Technol.*, vol. 20, no. 1, pp. 1–10, 2009.
- [18] D. L. Rudnick, R. E. Davis, and J. T. Sherman, “Spray underwater glider operations,” *J. Atmos. Ocean. Technol.*, vol. 33, pp. 1113–1122, Jun. 2016.
- [19] C. Qiu *et al.*, “Sea surface cooling in the Northern South China Sea observed using Chinese sea-wing underwater glider measurements,” *Deep-Sea Res. I, Oceanogr. Res. Papers*, vol. 105, pp. 111–118, Nov. 2015.
- [20] S. Ruiz, L. Renault, B. Garau, and J. Tintoré, “Underwater glider observations and modeling of an abrupt mixing event in the upper ocean,” *Geophys. Res. Lett.*, vol. 39, no. 1, pp. 1–7, 2012.
- [21] S. Fan and C. A. Woolsey, “Dynamics of underwater gliders in currents,” *Ocean Eng.*, vol. 84, pp. 249–258, Jul. 2014.

- [22] H. Huang, X. Y. Chen, Z. Zhou, Y. Xu, and C. Lv, "Study of the algorithm of backtracking decoupling and adaptive extended Kalman filter based on the quaternion expanded to the state variable for underwater glider navigation," *Sensors*, vol. 14, no. 12, pp. 23041–23066, 2014.
- [23] C. Shen et al., "Hybrid de-noising approach for fiber optic gyroscopes combining improved empirical mode decomposition and forward linear prediction algorithms," *Rev. Sci. Instrum.*, vol. 87, no. 3, pp. 033305-1–033305-8, 2016.
- [24] H. Huang, X. Chen, and J. Zhang, "Weight self-adjustment Adams implicit filtering algorithm for attitude estimation applied to underwater gliders," *IEEE Access*, vol. 4, no. 1, pp. 5695–5709, 2016.
- [25] W. Li, W. Wu, J. Wang, and L. Lu, "A fast SINS initial alignment scheme for underwater vehicle applications," *J. Navigat.*, vol. 66, no. 2, pp. 181–198, Mar. 2013.
- [26] W. Li, W. Wu, J. Wang, and M. Wu, "A novel backtracking navigation scheme for autonomous underwater vehicles," *Measurement*, vol. 47, pp. 496–504, Jan. 2014.
- [27] A. Noureldin, T. B. Karamat, M. D. Eberts, and A. El-Shafie, "Performance enhancement of MEMS-based INS/GPS integration for low-cost navigation applications," *IEEE Trans. Veh. Technol.*, vol. 58, no. 3, pp. 1077–1096, Mar. 2009.
- [28] H. Huang, X. Chen, B. Zhang, and J. Wang, "High accuracy navigation information estimation for inertial system using the multi-model EKF fusing adams explicit formula applied to underwater gliders," *ISA Trans.*, vol. 66, pp. 414–424, 2017.
- [29] S. J. Julier and J. K. Uhlmann, "Unscented filtering and nonlinear estimation," *Proc. IEEE*, vol. 92, no. 3, pp. 401–422, Mar. 2004.
- [30] D. Liu, J. Duan, and H. Shi, "A strong tracking square root central difference FastSLAM for unmanned intelligent vehicle with adaptive partial systematic resampling," *IEEE Trans. Intell. Transp. Syst.*, vol. 17, no. 11, pp. 3110–3120, Nov. 2016.
- [31] W. Li, J. Wang, L. Lu, and W. Wu, "A novel scheme for DVL-aided SINS in-motion alignment using UKF techniques," *Sensors*, vol. 13, no. 1, pp. 1046–1063, 2013.
- [32] B. Gao, S. Gao, Y. Zhong, G. Hu, and C. Gu, "Interacting multiple model estimation-based adaptive robust unscented Kalman filter," *Int. J. Control, Autom. Syst.*, vol. 15, no. 5, pp. 2013–2025, 2017.
- [33] J. Lim, "CDKF approach for estimating a static parameter of carrier frequency offset based on nonlinear measurement equations in OFDM systems," *Nonlinear Dyn.*, no. 78, pp. 703–711, 2014.
- [34] Z. Wang, X. Wang, Y. Liang, and F. Yang, "A new sigma-point filter-uniform random sampling Kalman filter," *IFAC-PapersOnLine*, vol. 50, no. 1, pp. 3853–3858, Jul. 2017.
- [35] C. Campestrini, T. Heil, S. Kosch, and A. Jossen, "A comparative study and review of different Kalman filters by applying an enhanced validation method," *J. Energy Storage*, vol. 8, pp. 142–159, Nov. 2016.
- [36] V. Bistrows and A. Kluga, "The analysis of the UKF-based navigation algorithm during GPS outage," *Elektronika Elektrotehnika*, vol. 19, no. 10, pp. 13–16, 2013.
- [37] G. Hu, S. Gao, and Y. Zhong, "A derivative UKF for tightly coupled INS/GPS integrated navigation," *ISA Trans.*, vol. 56, pp. 135–144, May 2015.
- [38] Y. Liu, X. Fan, C. Lv, J. Wu, L. Li, and D. Ding, "An innovative information fusion method with adaptive Kalman filter for integrated INS/GPS navigation of autonomous vehicles," *Mech. Syst. Signal Process.*, vol. 100, pp. 605–616, Feb. 2018.
- [39] B. Allotta, R. Costanzi, F. Fanelli, N. Monni, L. Paolucci, and A. Ridolfi, "Sea currents estimation during AUV navigation using Unscented Kalman Filter," *IFAC-PapersOnLine*, vol. 50, no. 1, pp. 13668–13673, Jul. 2017.
- [40] I. Arasaratnam and S. Haykin, "Cubature Kalman filters," *IEEE Trans. Autom. Control*, vol. 54, no. 6, pp. 1254–1269, Jun. 2009.
- [41] I. Arasaratnam, "Cubature Kalman filtering theory & applications," Ph.D. dissertation, Dept. Elect. Comput. Eng., McMaster Univ., Hamilton, ON, Canada, 2009.
- [42] I. Arasaratnam, S. Haykin, and T. R. Hurd, "Cubature Kalman filtering for continuous-discrete systems: Theory and simulations," *IEEE Trans. Signal Process.*, vol. 58, no. 10, pp. 4977–4993, Oct. 2010.
- [43] J. Liu, B. G. Cai, and J. Wang, "Cooperative localization of connected vehicles: Integrating GNSS with DSRC using a robust Cubature Kalman Filter," *IEEE Trans. Intell. Transp. Syst.*, vol. 18, no. 8, pp. 2111–2125, Aug. 2017.
- [44] Y. W. Zhao, "Performance evaluation of Cubature Kalman filter in a GPS/IMU tightly-coupled navigation system," *Signal Process.*, vol. 119, pp. 67–79, Feb. 2016.
- [45] J. Qin, Q. Ma, Y. Shi, and L. Wang, "Recent advances in consensus of multi-agent systems: A brief survey," *IEEE Trans. Ind. Electron.*, vol. 64, no. 6, pp. 4972–4983, Jun. 2017.
- [46] J. Qin, W. Fu, W. X. Zheng, and H. Gao, "On the bipartite consensus for generic linear multiagent systems with input saturation," *IEEE Trans. Cybern.*, vol. 47, no. 8, pp. 1948–1958, Aug. 2017.
- [47] J. Qin, Q. Ma, H. Gao, and W. X. Zheng, "Fault-tolerant cooperative tracking control via integral sliding mode control technique," *IEEE/ASME Trans. Mechatronics*, vol. 23, no. 1, pp. 342–351, Feb. 2018.
- [48] A. M. Bagirov and A. M. Rubinov, "Global optimization of marginal functions with applications to economic equilibrium," *J. Global Optim.*, vol. 20, pp. 215–237, Aug. 2001.
- [49] R. Horst, P. M. Pardalos, and N. V. Thoai, *Introduction to Global Optimization* 2nd ed. Amsterdam, The Netherlands: Kluwer, 2000.
- [50] S. Zhang, J. Yu, A. Zhang, and F. Zhang, "Spiraling motion of underwater gliders: Modeling, analysis, and experimental results," *Ocean Eng.*, vol. 60, pp. 1–13, Mar. 2013.



**HAOQIAN HUANG** received the bachelor's degree in automation from the China University of Mining and Technology, China, in 2007, the master's degree in agricultural mechanization engineering from Nanjing Agricultural University, China, in 2010, and the Ph.D. degree in instrument science and technology from Southeast University, China, 2015. From 2015 to 2017, he was a Post-Doctoral Researcher with Southeast University. He then joined Hohai University, China, where he has been an Assistant Professor with the School of Energy and Electrical Engineering since 2017. His main research interests include navigation technology applied to underwater glider, inertial navigation, and filtering methods. He received Bronze Medal at the 43th Geneva International Exhibition of Inventions for his Underwater Navigation System Design.



**JUN ZHOU** (M'03) received the B.S. degree in radio engineering from Sichuan University, Chengdu, China, the M.S. degree in information and control from Lanzhou University, Lanzhou, China, and the Ph.D. degree in electrical engineering from Kyoto University, Kyoto, Japan, respectively. He is currently a Professor with the Department of Automatic Control Engineering, Hohai University, Nanjing, China. His current research interests include nonlinear/hybrid systems and control, robustness performance synthesis, neural, multi-agent and distributed sensor networks, stabilization of multi-machine power systems, especially theoretical contributions are established in periodic systems, and control via harmonic analysis.



**JUN ZHANG** (S'12–M'13) received the B.S. degree in measurement and control technology and instrument from the Nanjing University of Science and Technology, Nanjing, China, in 2008, and the Ph.D. degree in instrument science and technology from Southeast University, Nanjing, China, in 2013, respectively. From 2013 to 2014, he was a Post-Doctoral Research Fellow with the Post-Doctoral Research Station of Control Science and Engineering, School of Automation, Southeast University. From 2014 to 2016, he was a Post-Doctoral Research Fellow with the Robotics Institute, Carnegie Mellon University. He is currently an Associate Researcher with the Robotic Sensor and Control Laboratory, School of Instrument Science and Engineering, Southeast University. His current research interests include bio-inspired robotics, mechatronics, multi-robot based microsystem assembly, and wireless sensor networks.



**YUAN YANG** received the B.S. and M.S. degrees in wireless communication from the China University of Mining and Technology, China, in 2007 and 2010, and the Ph.D. degree from the Institute of Computer Science, Freie Universitaet Berlin, Germany, in 2015. Since 2015, she has been with the School of Instrument Science and Engineering, Southeast University, China. Her research interests include non-parametric statistics, parameter estimation, indoor localization, and wireless sensor networks. Her further work will investigate distributed positioning and target tracking and positioning on indoor mobile robots and drones.



**RUI SONG** was born in 1991. He received the B.Sc. degree in automatic control from the College of Electrical Engineering, Anhui Polytechnic University, Wuhu, China. He is currently pursuing the Ph.D. with the Key Laboratory of Micro-Inertial Instrument and Advanced Navigation Technology, School of Instrument Science and Engineering, Southeast University, China. He was a Research Student with the University of Birmingham, U.K., for one year, where he was mainly engaged in

the projects that funded by Microwave Integrated System Laboratory and Jaguar Land Rover. He has published several papers and holds patents in the fields, such as inertial instrument modeling, artificial intelligent algorithms, and navigation methods. His research interests are inertial measurement, integrated navigation system, and information fusion.



**JIANFENG CHEN** received the bachelor's degree in industry automation and the master's degree in power electronics and power drives from Jiangsu University in 2002 and 2005, respectively, and the Ph.D. degree in instrument science and technology from Southeast University in 2015. He is currently an Associate Professor with the Automotive Engineering Research Institute, Jiangsu University, China. His professional activities mainly span SINS algorithm design and evaluation, data fusion algorithms, state estimation, performance analysis, and control optimization of vehicle motion. His current research interests include strapdown inertial navigation system (SINS), SINS/GNSS integrated measurement, and vehicle dynamic and control.



**JIAJIN ZHANG** received the B.E. degree in engineering of surveying and mapping from the Shandong University of Technology in 2004 and the M.E. degree in photogrammetric engineering and remote sensing from Wuhan University, China, in 2006. His research interests include marine surveying and mapping work and quantitative remote sensing study.

...